Journal of Thermal Analysis and Calorimetry (2021) 144:2515–2523
https://doi.org/10.1007/s10973-020-10054-w

Potential energy and atomic stability of H_2O/CuO nanoparticles flow and heat transfer in non-ideal microchannel via molecular dynamic approach: the Green–Kubo method

Yuanzhou Zheng[1,2] · Xinzhu Zhang[1,2] · Mohammad Taghi Soleimani Mobareke[3] · Maboud Hekmatifar[3] · Arash Karimipour[4] · Roozbeh Sabetvand[5]

Received: 7 May 2020 / Accepted: 6 July 2020 / Published online: 30 July 2020

Abstract
It is interesting to investigate the number of nanoparticle (NP) and temperature effects on H_2O/CuO nanofluid thermal conductivity and the atomic manner in a non-ideal microchannel. The outcomes of the physical features of these structures were supposed using molecular dynamic (MD) method and LAMMPS simulation package. For the study of dynamic properties of nanofluid microchannel system, parameters such as temperature profiles, velocity, density, and potential energy of H_2O/CuO atomic structures were calculated. Furthermore, the thermal conductivity of these structures was estimated by the Green–Kubo method in the final step. This simulation shows that nanoparticle number is a crucial parameter in nanofluid movement in a microchannel. Theoretically, via adding CuO nanoparticle to H_2O fluid, the maximum rate of velocity, density, temperature, and thermal conductivity of base fluid increases to 0.106 g cm^{-3}, 29.810 A ps^{-1}, 549.217 K, and 0.81 W mK^{-1} rates, respectively. Moreover, the temperature increase of Cu microchannel increases the rate of density, velocity, temperature, and thermal conductivity of CuO nanofluids.

Keywords MD · Water/copper oxide · Microchannel · Green–Kubo method

Introduction

In engineering and physics, fluid dynamics is a subcategory of fluid mechanics which explains the fluids flow. It contains some categories, such as aerodynamics and hydrodynamics [1–4]. Fluid dynamics contains a large variety of uses, like computing moments and forces on aircraft, verifying the mass flow rate of petroleum by pipelines, forecasting the patterns of weather, knowing about nebulae in interstellar space, and modeling fission weapon explosion [5–8]. Fluid dynamics proposes a well-organized structure which contains empirical and semiempirical laws that came from flow measurement and used for solving practical problems [9, 10]. The way to solve the problem of fluid dynamics usually entails the calculation of different features of the fluid, like pressure, flow velocity, density, temperature, and thermal conductivity, as functions of time and space [11, 12]. More, the nanofluid, described as a fluid with nanosized solids, the "nanoparticles (NPs)." The NP colloidal suspensions are formed by these liquids [13, 14]. CNTs, silicon carbides, metals, and oxides are the elements of NPs that were used in nanofluids. Water molecules and oil are typical cases of base fluids [15]. Ingenious aspects of nanofluids make them conceivably potent for lots of operations in heat transmitting, as in machining, chillers, fridges, electronic cooling systems, microelectronics, and fuel cells [16, 17]. Nanofluids, compared to typical liquids, point out better thermic power

✉ Arash Karimipour
arashkarimipour@tdtu.edu.vn

1 Hubei Key Laboratory of Inland Shipping Technology, Wuhan University of Technology, 588 Youyi Avenue, Wuhan, China

2 School of Navigation, Wuhan University of Technology, 588 Youyi Avenue, Wuhan, China

3 Department of Mechanical Engineering, Khomeini Shahr University, Esfahan, Iran

4 Sustainable Management of Natural Resources and Environment Research Group, Faculty of Environment and Labour Safety, Ton Duc Thang University, Ho Chi Minh City, Vietnam

5 Department of Energy Engineering and Physics, Faculty of Condensed Matter Physics, Amirkabir University of Technology, Tehran, Iran

of convicted and conducting heat transmitting efficiency [18–20]. The primary researches demonstrate that appreciable increase in nanofluid thermal features than the base fluid, especially the heat transmission coefficient, has been mainly discredited. In spite of definitive experimental investigations, theoretical papers keep on following the claim of anomalous enhancement, especially by Brownian and thermophoretic mechanisms, as proposed by Buongiorno [21–27]. The molecular dynamic (MD) technique is another way to nanofluid studies. The MD technique is the greatest crucial class of computer simulation which is able to predict the atomic manner of framework assortment [28–30]. Today, this estimation technique is broadly applied in the thermal study of atomic structures [31, 32]. In this work, theoretical calculations were performed to predict nanoparticle number and microchannel temperature effect on the dynamic manner of H_2O/CuO nanofluid.

Computational method

In the current numerical study, the MD method was used to study H_2O/CuO nanofluid inside a non-ideal microchannel. The MD method is a computational approach to trace dynamic movements of atoms. In this method, the interaction of atoms with one another is permitted, so it gives the system's mechanical development concept. In the present study, every MD simulation was done by applying the LAMMPS package released by laboratories [33–36]. This software expansion started during the 1990s was supported by a unified research and expansion concurrence (CRADA) between Dupont firms, Bristol Myers Squibb, and Sandia and LLNL laboratories and Cray. For using this simulation package to predict H_2O/CuO nanofluid, the first Cu non-ideal microchannel was simulated at $T = 300$ K. In the next step, H_2O fluid with differing numbers of CuO NPs was simulated and have these atomic structures settled in the microchannel center [37–43]. The primary atomic pattern was fulfilled by Packmol software [44]. Figure 1 indicates a simulation box at perspective, front, and top faces that was seen by OVITO (Open Visualization Tool) software [45]. OVITO is a scientific visualization and analysis package for molecule- and atom-based simulation data [46, 47].

In current MD simulations, periodic boundary statuses were fulfilled in whole 3 directions. To create the first status, the Nose–Hoover thermostat was used for atoms in the simulation box for fixed temperature at 300 K with one femtosecond time step [48, 49]. In the 2nd phase, extrinsic force equaled with $F_{ext} = 0.02$ eV A^{-1} entered to fluid and the microcanonical ensemble was applied for estimating the dynamic manner of H_2O in Cu microchannel [50]. Numerical researches for H_2O molecules usually use simple experiential models [51–54]. Then, simulations are able to

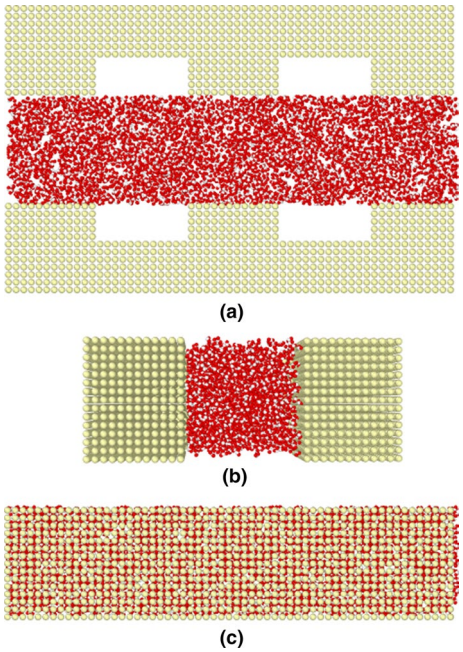

Fig. 1 Schematic picture of Cu microchannel and H_2O fluid designed by Packmol software at **a** perspective, **b** front, and **c** top views

calculate features of H_2O molecules that are used to compare with experiential reports. The most usual procedures for the MD simulation of H_2O molecules include SPC, TIP3P, and TIP4P types. In total, 3–5 interaction spots were fulfilled in these models [55–57]. At SPC type 3, sites that were fulfilled for positive charges and electrostatic interactions on H atoms were balanced via a properly negative charge that added to oxygen atom [58]. Moreover, via a Lennard-Jones (LJ) potential with only one lone interaction point per molecule centered on the O atom, the no bonded interaction between 2 H_2O molecules was simulated. The Lennard-Jones potential can be defined as a mathematically uncomplicated formula that estimates the interaction between particles (molecules or atoms) [59]. John Lennard-Jones was the first person who suggested a form of this interatomic potential in 1924 [60]. The commonest formula for LJ potential is:

$$U(r) = 4\varepsilon\left[\left(\frac{\sigma}{r_{ij}}\right)^{12} - \left(\frac{\sigma}{r_{ij}}\right)^{6}\right] \quad r \ll r_c \tag{1}$$

In current equation, the depth of potential is shown by ε, and σ is the distance, when potential is zero, and also, the distance between 2 particles is r_{ij}. In the MD simulations, the two σ and ε factors are depended on the kind of atoms in the box. The following simple harmonic oscillator equations show angle stretch and bond in this atomic pattern [61]:

$$E_r = \frac{1}{2}k_r(r - r_0) \tag{2}$$

$$E_\theta = \frac{1}{2}k_\theta(\theta - \theta_0) \tag{3}$$

where r_0 and θ_0 are the atomic bond length and angles balanced value, individually. K_r and K_θ are harmonic oscillator constants. At the SPC pattern, the θ_0 of HOH angle equals 109.47°, while the r_0 of OH bond is equivalent to 1.0 A, and. Furthermore, all interatomic interactions involving the hydrogen atoms are ignored. This model and other parameters for H_2O molecule simulation are presented in Table 1 [58].

To study nanoparticles added to base fluid, CuO nanoparticles are simulated. The atomic structure of H_2O/CuO nanofluid atomic structures is depicted in Fig. 2. To simulate CuO nanoparticles, there are also several atomic potentials such as UFF, dreiding, and Tersoff potentials [62]. Among the interatomic potentials, the best selection for simulating metal oxide structures is Tersoff potential. The most familiar interpretation of the Tersoff potential is [63],

$$E = \frac{1}{2}\sum_{i}\sum_{i\neq j} V_{ij} \tag{4}$$

$$V_{ij} = f_C(r_{ij})\left[f_R(r_{ij}) + b_{ij}f_A(r_{ij})\right] \tag{5}$$

In this equation, f_R is a two-body term, and f_A includes three-body interactions. The summations in the formula are over whole neighbors' J and K of atom I within a cutoff distance = $R + D$ [64]. In the last part of the simulations, after determining the interatomic potentials and atomic structure, to investigate the flow mechanical behavior in the Copper microchannel, temperature profiles, velocity, and the density are calculated. In the end, the thermal conductivity of atomic structures by the Green–Kubo method was calculated [65].

Results and discussion

Potential energy of atomic structures

In the initial phase of the molecular dynamic simulation, the atomic patterns' potential energy was examined to ensure the stability of this MD simulation. Figures 3 and 4 show that one ns time is sufficient for equilibration of fluid/nanofluid and microchannel structures. Figure 3 shows that the potential energy and atomic stability of the simulated system

Table 1 Length and energy specifications for Lennard-Jones potential for the SPC pattern of H_2O molecules [58]

Element	ε/kcal mol^{-1}	σ/A^{-1}
O	0.1553	3.166
H	0.0000	0.000

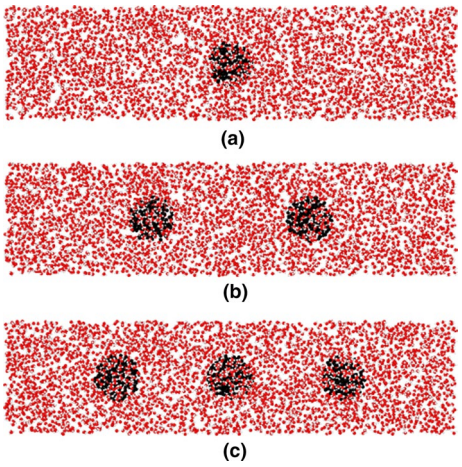

Fig. 2 Schematic of H_2O/CuO nanofluid with **a** one, **b** two, and **c** three CuO NPs

increases by adding nanoparticle to the base fluid. Furthermore, the temperature of microchannel increasing does not have an appreciable effect on the stability of atomic structures. After verifying the potential energy equilibration, temperature profiles, velocity, and the density of fluid/nanofluid structures in the next steps were reported.

Density profile of atomic structures

The density profiles indicate fluid–particle interactions with the microchannel walls, so this parameter is so important. To calculate the density profile, the microchannel is divided into 2226 bins along the y direction, and every bin has $L_x * L_z * \Delta y$ vol., where the microchannel lengths are L_z and L_x together with z and x directions, and L_y/N_{bin} refers to Δy. Figure 5 displays the dispersion of fluid atoms in the microchannel at which the temperature of simulated walls is fixed at 300 K. It is obvious that the fluid atoms are absorbed

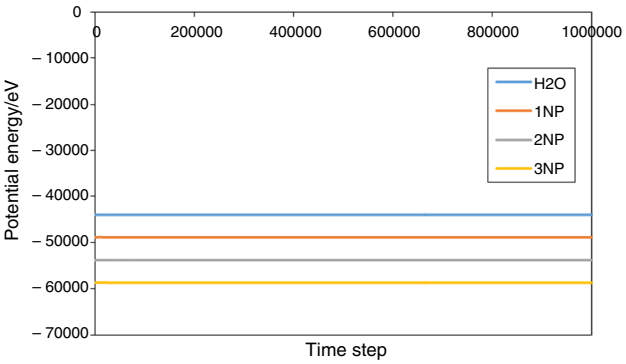

Fig. 3 Potential energy of H_2O molecules and H_2O/CuO nanofluid with a varied number of NPs being the simulation time phase function

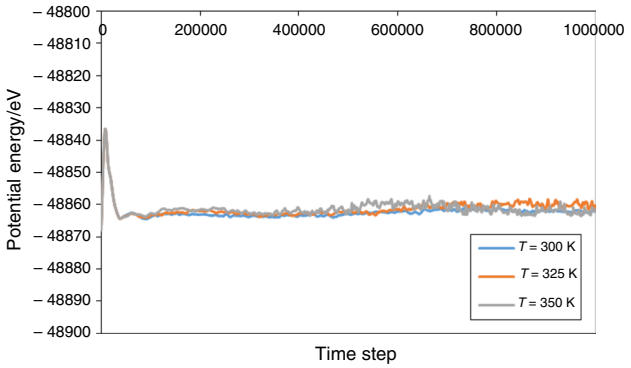

Fig. 4 Potential energy of H_2O/CuO nanofluid with one nanoparticle being the microchannel temperature and simulation time phase function

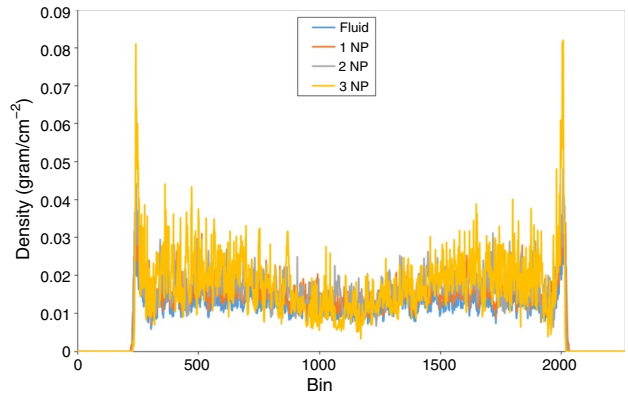

Fig. 5 Density profile of fluid/nanofluid being the CuO nanoparticles number function

via the nanochannel surface and decrease the density profile of these atomic patterns in the middle of Cu microchannel. Via adding CuO NPs to H_2O liquid, the density profile of structure rises. Further, it can be concluded that the nanoparticle numbers have important influence on the distributions of nanofluid atom positions and nanofluid density increases from 0.030 to 0.081 g cm^{-3} by adding 3 CuO nanoparticles to H_2O fluid (see Table 2). Furthermore, by increasing temperature from 300 to 325 K and 350 K, the density maximum rate reaches 0.062 g cm^{-3} and 0.106 g cm^{-3}, individually (Fig. 6 and Table 3). Therefore, the temperature of Cu microchannel is another important parameter for the dynamic manner of nanofluid, which should be considered in practical applications.

Velocity profile of atomic structures

The velocity profiles of nanofluid structure indicate how these atomic structures move being the simulation time function. To calculate the velocity dispersion of fluid/

Table 2 Density maximum rate in fluid/nanofluid by a varied number of CuO NPs

Sample	Density/g cm^{-3}
H_2O fluid	0.030
H_2O fluid with 1 NP	0.036
H_2O fluid with 2 NPs	0.048
H_2O fluid with 3 NPs	0.081

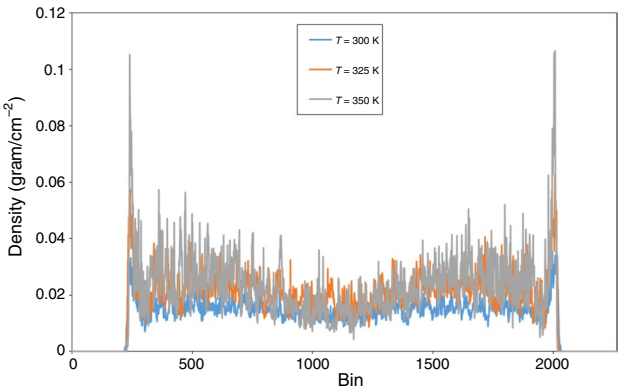

Fig. 6 Density profile of H_2O/CuO nanofluid with one nanoparticle as a function of Cu microchannel temperature

Table 3 Density maximum rate in H_2O/CuO nanofluid with one nanoparticle at various temperatures

Temperature/K	Density/g cm^{-3}
300	0.036
325	0.062
350	0.106

nanofluid atoms in a microchannel, the simulation box is divided into 2226 bins in the *y* direction. Figure 7 displays the velocity distribution of fluid and nanofluid with various numbers of nanoparticles in Cu microchannel. It can be seen that the velocity rate is minimum near the microchannel wall surface. It happens because of the strong interactions between wall atoms and nanofluid particles. Furthermore, this physical parameter becomes maximized in the middle region of microchannel, which shows the Poiseuille flow manner of fluid/nanofluid particles in a non-ideal microchannel. Based on these calculated results, the maximum rate of fluid velocity is 3.609 A ps^{-1}, and by adding 3 NPs to fluid–structure, this parameter rises to 27.100 A ps^{-1} (Table 4). Microchannel temperature increasing has an identical effect on the dynamic manner of nanofluid. By temperature increasing from 300 to 350 K, the maneuverability of the atomic structure grows

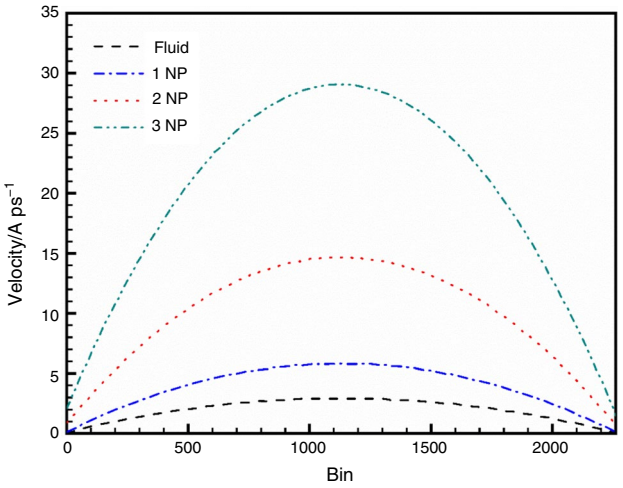

Fig. 7 Velocity profile of fluid/nanofluid being the CuO NP number function

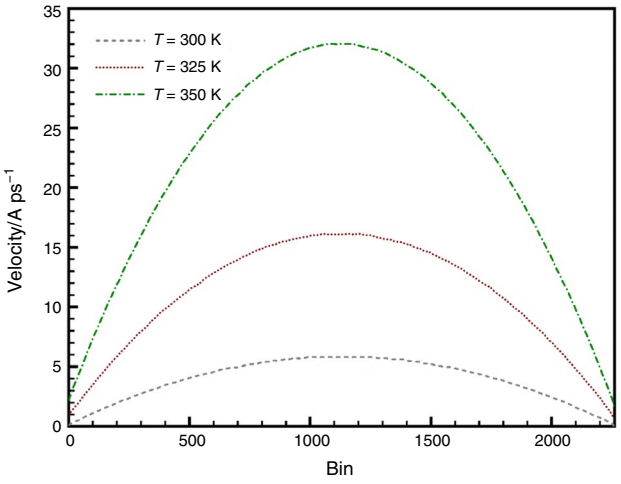

Fig. 8 Velocity profile of H_2O/CuO nanofluid with one nanoparticle as a function of Cu microchannel temperature

Table 4 Atomic velocity maximum rate in fluid/nanofluid by a varied number of CuO NPs

Sample	Velocity/A ps^{-1}
H_2O fluid	3.609
H_2O fluid with 1 NP	7.218
H_2O fluid with 2 NPs	13.678
H_2O fluid with 3 NPs	27.100

Table 5 Atomic velocity maximum rate in H_2O/CuO nanofluid with one nanoparticle at various temperatures

Temperature/K	Velocity/A ps^{-1}
300	7.218
325	15.046
350	29.810

by ½ $mv^2 = 3/2kT$ equation. Numerically, the atomic velocity maximum rate grows from 7.218 to 27.100 A ps^{-1}. Figure 8 shows the velocity variation of fluid/nanofluid structures as a function of simulation temperature (Table 5). Based on this figure, it can be said that, by increasing the temperature, the effective force enforced to nanofluid from microchannel walls grow less, and the atomic velocity of H_2O/CuO nanofluids increases.

Temperature profile of atomic structures

The thermodynamic features of atomic patterns have a direct impact on the function in practical use. In this part, it was examined how the fluid/nanofluid atom temperature is dispersed in simulated Cu microchannels. To attain the temperature profile, the average temperature is computed in every 2226 bin and in every 100-time steps. Figures 9 and 10 show the effects of nanoparticle and microchannel temperature on fluid/nanofluid temperature profiles along the width of the microchannel. As presented in these figures, the Poiseuille flow has a quadratic temperature profile, and the temperature maximum rate happens in the center of a microchannel. Figure 9 demonstrates the atomic temperature

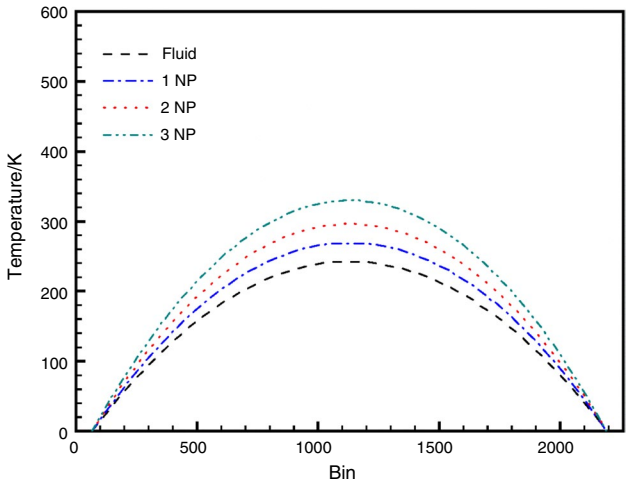

Fig. 9 Temperature profile of fluid/nanofluid as a function of CuO nanoparticles number

of fluid/nanofluid structures grow via CuO nanoparticle adding to H_2O molecules. This phenomenon occurs because of nanoparticle high thermal conductivity rather than base fluid. From numerically view, the maximum rate of temperature differs from 407.345 to 499.289 K via growth in CuO

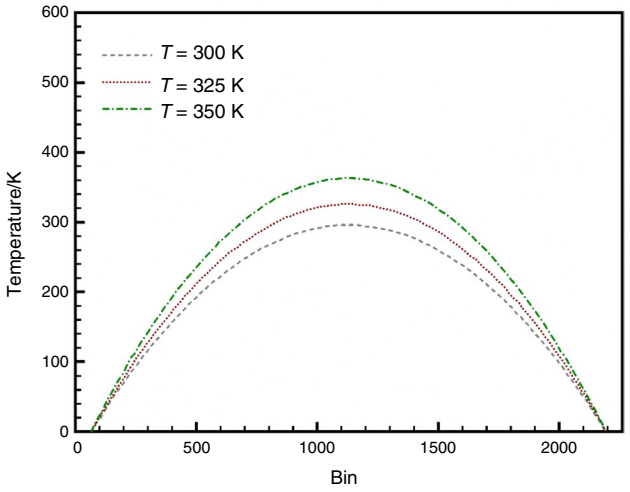

Fig. 10 Temperature profile of H_2O/CuO nanofluid with one nanoparticle as a function of temperature

Table 6 Atomic temperature maximum rate in fluid and nanofluid by varied number of CuO nanoparticles

Sample	Fluid/nanofluid temperature/K
H_2O fluid	366.610
H_2O fluid with 1 NP	407.345
H_2O fluid with 2 NPs	448.080
H_2O fluid with 3 NPs	499.289

Table 7 Atomic temperature maximum rate in nanofluid at varied temperatures

Sample temperature/K	Nanofluid temperature/K
300	448.080
325	492.887
350	549.217

NPs from 1–3 numbers, as given in Table 6. Microchannel temperature increasing has an alike impact on fluid/nanofluid atomic temperature profile, being presented in Fig. 10. Via growth in microchannel wall temperature from 300 to 350 K, the nanofluid temperature maximum rate grows from 448.080 to 549.217 K (Table 7). The fast transfer of temperature from the microchannel walls to the simulated nanofluids at higher temperatures causes this phenomenon.

Thermal conductivity of atomic structures

At the final step, the MD simulations are used for estimating the thermal conductivity of H_2O/CuO nanofluid. Before calculating nanofluid thermal conductivity, the thermal conductivity of H_2O molecules is calculated. Thermal conductivity of simulated structures is estimated via Green–Kubo formalism based on the fixed number of energy condition, volume, and atoms [31, 66]:

$$k = \frac{1}{3k_B VT^2}\int_0^\infty < S(t)\cdot S(0) > \mathrm{d}t \tag{6}$$

where T is temperature, V is the simulation volume, k_B is the Boltzmann constant, and S is the heat current vector with elements in X–Y–Z directions. The heat current S is estimated in every time phase by applying velocity and the stress tensor of every atom in LAMMPS. $<S(t).S(0)>$ is named the function of heat current autocorrelation, which is the correlation of the heat current at different times. The calculated rate for the thermal conductivity of H_2O molecules is 0.62 W mK^{-1}, where this rate is appropriate for experimental value (0.59 W mK^{-1}) [32]. Table 8 shows that the thermal conductivity of H_2O/CuO nanofluid increases by inserting CuO nanoparticle to base fluid. Numerically, by CuO nanoparticle adding to H_2O molecules, the thermal conductivity of nanofluid rises to 0.75 W mK^{-1}. Furthermore, the thermal conductivity of H_2O/CuO nanofluid increases from 0.68 to 0.81 W mK^{-1} by microchannel temperature increasing from 300 to 350 K (Table 9). This thermal manner of nanofluid arises from the increase in the mobility of nanofluid atoms by microchannel temperature rising.

Table 8 Thermal conductivity of fluid and nanofluid by various CuO nanoparticle numbers

Sample	Thermal conductivity/W mK^{-1}
H_2O fluid	0.62
H_2O fluid with 1 NP	0.68
H_2O fluid with 2 NPs	0.71
H_2O fluid with 3 NPs	0.75

Table 9 Thermal conductivity of nanofluid structure with one CuO nanoparticle at various temperatures

Sample temperature/K	Thermal conductivity/W mK^{-1}
300	0.68
325	0.74
350	0.81

Conclusions

In the present study, the MD simulation is used for estimating the dynamic and thermal manner of H_2O/CuO nanofluid in the non-ideal microchannel at 300 K, 325 K, and 350 K temperatures. In current simulations, the number of CuO NPs differs from 1 to 3 NPs [67, 68]. These conclusions from stated simulations are:

(A) The number of CuO NPs inside the base fluid is a prominent factor in H_2O/CuO nanofluid density. In the simulated models, the density of H_2O/CuO nanofluid increased from 0.036 to 0.081 g cm^{-3} with an increase in the number of nanoparticles from 1–3, respectively.
(B) The MD results propose that the atomic density of H_2O/CuO density is increased by increasing the microchannel temperature from 300 to 350 K.
(C) In simulated structure, the atomic velocity of nanofluid has a straight connection with CuO NP number. The maximum rate of velocity in H_2O/CuO nanoparticle raises to 27.100 A ps^{-1} via adding 3 NPs to base fluid.
(D) Maximum velocity of simulated nanofluid increases from 7.218 to 29.810 A ps^{-1} via temperature growth in microchannel temperature from 300 to 350 K.
(E) By CuO nanoparticle adding to base fluid, the atomic temperature of nanofluid grows. Theoretically, the maximum temperature of nanofluid increases from 407.345 to 499.289 K by 1–3 CuO nanoparticle, adding to H_2O molecules.
(F) By temperature increasing in simulated Cu microchannel, the maximum rate of nanofluid temperature reaches 549.217 K.
(G) Thermal conductivity of H_2O/CuO nanofluid increases to 0.75 W mK^{-1} by 3 CuO nanoparticle, adding to H_2O molecules.
(H) The thermal conductivity of H_2O/CuO nanofluid changes from 0.68 to 0.81 W mK^{-1} by temperature increasing from 300 to 350 K.

Acknowledgements This work was supported by the National Natural Science Foundation of China (Grant Number 51979215).

References

1. Hoseinzadeh S, Heyns PS. Thermo-structural fatigue and lifetime analysis of a heat exchanger as a feedwater heater in power plant. Eng Fail Anal. 2020. https://doi.org/10.1016/j.engfailanal.2020.104548.
2. Hoseinzadeh S, et al. A detailed experimental airfoil performance investigation using an equipped wind tunnel. Flow Meas Instrum. 2020. https://doi.org/10.1016/j.flowmeasinst.2020.101717.
3. Hoseinzadeh S, et al. Numerical validation heat transfer of rectangular cross-section porous fins. J Thermophys Heat Transf. 2019;33(3):698–704. https://doi.org/10.2514/1.T5583.
4. Hoseinzadeh S, et al. The injection of Ag nanoparticles on surface of WO 3 thin film: enhanced electrochromic coloration efficiency and switching response. J Mater Sci Mater Electron. 2017;28(19):14855–63. https://doi.org/10.1007/s10854-017-7357-9.
5. Ghalambaz M, et al. Melting of nanoparticles-enhanced phase-change materials in an enclosure: effect of hybrid nanoparticles. Int J Mech Sci. 2017;134:85–97. https://doi.org/10.1016/j.ijmecsci.2017.09.045.
6. Ghalambaz M, et al. Fluid-structure interaction study of natural convection heat transfer over a flexible oscillating fin in a square cavity. Int J Therm Sci. 2017;111:256–73. https://doi.org/10.1016/j.ijthermalsci.2016.09.001.
7. Ghalambaz M, et al. Phase-change heat transfer in a cavity heated from below: the effect of utilizing single or hybrid nanoparticles as additives. J Taiwan Inst Chem Eng. 2017;72:104–15. https://doi.org/10.1016/j.jtice.2017.01.010.
8. Ghalambaz M, et al. Effects of nanoparticles diameter and concentration on natural convection of the Al_2O_3–water nanofluids considering variable thermal conductivity around a vertical cone in porous media. Adv Powder Technol. 2015;26(1):224–35. https://doi.org/10.1016/j.apt.2014.10.001.
9. Ghasemi MH, et al. Numerical analysis of non-fourier heat transfer in a solid cylinder with dual-phase-lag phenomenon. CMES Comput Model Eng Sci. 2020. https://doi.org/10.32604/cmes.2020.07827.
10. Bahrami A, et al. Experimental investigation of co-flow jet's airfoil flow control by hot wire anemometer. Rev Sci Instrum. 2019;90(12):125107. https://doi.org/10.1063/1.5113592.
11. Sohani A, et al. Determination of Hildebrand solubility parameter of pure 1-alkanols up to high pressures. J Mol Liq. 2020;297:111847. https://doi.org/10.1016/j.molliq.2019.111847.
12. Goodarzi M, et al. Investigation of nanofluid mixed convection in a shallow cavity using a two-phase mixture model. Int J Therm Sci. 2014;75:204–20. https://doi.org/10.1016/j.ijthermalsci.2013.08.003.
13. Taylor R, et al. Small particles, big impacts: a review of the diverse applications of nanofluids. J Appl Phys. 2013;113(1):1. https://doi.org/10.1063/1.4754271.
14. Buongiorno J. Convective transport in nanofluids. J Heat Transfer. 2006;128:240–50. https://doi.org/10.1115/1.2150834.
15. Argonne Transportation Technology R&D Center.
16. Minkowycz WJ, et al. Nanoparticle heat transfer and fluid flow, vol. 4. Boca Raton: CRC Press; 2012.
17. Das SK, Choi SUS, Wenhua Y, Pradeep T. Nanofluids: science and technology. Hoboken: Wiley; 2007. p. 397.
18. Kakaç S, Pramuanjaroenkij A. Review of convective heat transfer enhancement with nanofluids. Int J Heat Mass Transf. 2009;52(13-14):3187–96. https://doi.org/10.1016/j.ijheatmasstransfer.2009.02.006.
19. Witharana S, Ding Y. Stability of nanofluids in quiescent and shear flow fields. Nanoscale Res Lett. 2011;6:231.
20. Chen H, et al. Predicting thermal conductivity of liquid suspensions of nanoparticles (nanofluids) based on rheology. Particuology. 2009;7(2):151–7. https://doi.org/10.1016/j.partic.2009.01.005.
21. Bahiraei M. Effect of particle migration on flow and heat transfer characteristics of magnetic nanoparticle suspensions. J Mol Liq. 2015;209:531–8. https://doi.org/10.1016/j.molliq.2015.06.030.
22. Malvandi A, et al. Thermal performance analysis of hydromagnetic Al2O3-water nanofluid flows inside a concentric microannulus considering nanoparticle migration and asymmetric heating.

Int J Therm Sci. 2016;109:10–22. https://doi.org/10.1016/j.ijthermalsci.2016.05.023.
23. Bahiraei M. Studying nanoparticle distribution in nanofluids considering the effective factors on particle migration and determination of phenomenological constants by Eulerian-Lagrangian simulation. Adv Powder Technol. 2015;26(3):802–10. https://doi.org/10.1016/j.apt.2015.02.005.
24. Pakravan HA, Yaghoubi M. Analysis of nanoparticles migration on natural convective heat transfer of nanofluids. Int J Therm Sci. 2013;68:79–93. https://doi.org/10.1016/j.ijthermalsci.2012.12.012.
25. Malvandi A, et al. Two-component heterogeneous mixed convection of alumina/water nanofluid in microchannels with heat source/sink. Adv Powder Technol. 2016;27(1):245–54. https://doi.org/10.1016/j.apt.2015.12.009.
26. Malvandi A, Ganji DD. Brownian motion and thermophoresis effects on slip flow of alumina/water nanofluid inside a circular microchannel in the presence of a magnetic field. Int J Therm Sci. 2014;84:196–206. https://doi.org/10.1016/j.ijthermalsci.2014.05.013.
27. Bahiraei M, Abdi F. Development of a model for entropy generation of water-TiO2 nanofluid flow considering nanoparticle migration within a minichannel. Chemometr Intell Lab Syst. 2016;157:16–28. https://doi.org/10.1016/j.chemolab.2016.06.012.
28. Alder BJ, Everett Wainwright T. Studies in molecular dynamics. I. General method. J Chem Phys. 1959;31(2):459–66. https://doi.org/10.1063/1.1730376.
29. Rahman A. Correlations in the motion of atoms in liquid argon. Phys Rev. 1964;136(2A):A405. https://doi.org/10.1103/PhysRev.136.A405.
30. Laplace PS. Théorie analytique des probabilités. Paris: Courcier; 1820.
31. Kubo R. Statistical-mechanical theory of irreversible processes. I. General theory and simple applications to magnetic and conduction problems. J Phys Soc Jpn. 1957;12(6):570–86. https://doi.org/10.1143/jpsj.12.570.
32. Touloukian P, Ho K. Purdue Research Foundation, TPRC Data Series vol 3 (1970) https://apps.dtic.mil/dtic/tr/fulltext/u2/a951937.pdf.
33. Plimpton S. Fast parallel algorithms for short-range molecular dynamics. No. SAND-91-1144. Sandia National Labs., Albuquerque, NM (United States), 1993. https://doi.org/10.1006/jcph.1995.1039.
34. Plimpton SJ, Thompson AP. Computational aspects of many-body potentials. MRS Bull. 2012;37(5):513. https://doi.org/10.1557/mrs.2012.96.
35. Brown WM, et al. Implementing molecular dynamics on hybrid high performance computers–short range forces. Comput Phys Commun. 2011;182(4):898–911. https://doi.org/10.1016/j.cpc.2010.12.021.
36. Brown WM, et al. Implementing molecular dynamics on hybrid high performance computers–particle–particle particle-mesh. Comput Phys Commun. 2012;183(3):449–59. https://doi.org/10.1016/j.cpc.2011.10.012.
37. Sarafraz MM, et al. Thermal performance of a heat sink microchannel working with biologically produced silver-water nanofluid: experimental assessment. Exp Thermal Fluid Sci. 2018;91:509–19. https://doi.org/10.1016/j.expthermflusci.2017.11.007.
38. Sarafraz MM, et al. Reforming of methanol with steam in a micro-reactor with Cu–SiO2 porous catalyst. Int J Hydrogen Energy. 2019;44(36):19628–39. https://doi.org/10.1016/j.ijhydene.2019.05.215.
39. Sarafraz MM, et al. Experimental investigation and performance optimisation of a catalytic reforming micro-reactor using response surface methodology. Energy Convers Manag. 2019;199:111983. https://doi.org/10.1016/j.enconman.2019.111983.
40. Sarafraz MM, et al. Fouling formation and thermal performance of aqueous carbon nanotube nanofluid in a heat sink with rectangular parallel microchannel. Appl Therm Eng. 2017;123:29–39. https://doi.org/10.1016/j.applthermaleng.2017.05.056.
41. Sarafraz MM, Arjomandi M. Thermal performance analysis of a microchannel heat sink cooling with copper oxide-indium (CuO/In) nano-suspensions at high-temperatures. Appl Therm Eng. 2018;137:700–9. https://doi.org/10.1016/j.applthermaleng.2018.04.024.
42. Sarafraz MM, Arjomandi M. Demonstration of plausible application of gallium nano-suspension in microchannel solar thermal receiver: experimental assessment of thermo-hydraulic performance of microchannel. Int Commun Heat Mass Transfer. 2018;94:39–46. https://doi.org/10.1016/j.icheatmasstransfer.2018.03.013.
43. Sarafraz MM, et al. Thermal and hydraulic analysis of a rectangular microchannel with gallium-copper oxide nano-suspension. J Mol Liq. 2018;263:382–9. https://doi.org/10.1016/j.molliq.2018.05.026.
44. Martínez L, et al. PACKMOL: a package for building initial configurations for molecular dynamics simulations. J Comput Chem. 2009;30(13):2157–64. https://doi.org/10.1002/jcc.21224.
45. Stukowski A. Visualization and analysis of atomistic simulation data with OVITO–the open visualization tool. Modell Simul Mater Sci Eng. 2009;18(1):015012. https://doi.org/10.1088/0965-0393/18/1/015012.
46. Safaei MR, et al. Investigation of heat transfer enhancement in a forward-facing contracting channel using FMWCNT nanofluids. Numer Heat Transf A Appl. 2014;66(12):1321–40. https://doi.org/10.1080/10407782.2014.916101.
47. Dehghani Y, et al. Experimental investigation toward obtaining a new correlation for viscosity of WO_3 and Al_2O_3 nanoparticles-loaded nanofluid within aqueous and non-aqueous base-fluids. J Therm Anal Calorim. 2019;135(1):713–28. https://doi.org/10.1007/s10973-018-7394-5.
48. Nosé S. A unified formulation of the constant temperature molecular dynamics methods. J Chem Phys. 1984;81(1):511–9. https://doi.org/10.1063/1.447334.
49. Hoover WG. Canonical dynamics: equilibrium phase-space distributions. Phys Rev A. 1985;31(3):1695. https://doi.org/10.1103/PhysRevA.31.1695.
50. Gibbs JW. Elementary principles in statistical mechanics. New York: Charles Scribner's Sons; 1902.
51. Du C, et al. Thermal conductivity enhancement of nanofluid by adding multiwalled carbon nanotubes: characterization and numerical modeling patterns. Math Methods Appl Sci. 2020. https://doi.org/10.1002/mma.6466.
52. Xu Y, et al. Synthesis and characterization of additive graphene oxide nanoparticles dispersed in water: experimental and theoretical viscosity prediction of non-Newtonian nanofluid. Math Methods Appl Sci. 2020. https://doi.org/10.1002/mma.6381.
53. Liu WI, et al. A novel comprehensive experimental study concerned graphene oxide nanoparticles dispersed in water: synthesise, characterisation, thermal conductivity measurement and present a new approach of RLSF neural network. Int Commun Heat Mass Transf. 2019;109:104333. https://doi.org/10.1016/j.icheatmasstransfer.2019.104333.
54. Karimipour A, et al. Thermal conductivity enhancement via synthesis produces a new hybrid mixture composed of copper oxide and multi-walled carbon nanotube dispersed in water: experimental characterization and artificial neural network modeling. Int J Thermophys. 2020;41(8):116. https://doi.org/10.1007/s10765-020-02702-y.

55. Arasteh H, et al. Optimal arrangements of a heat sink partially filled with multilayered porous media employing hybrid nanofluid. J Therm Anal Calorim. 2019;137(3):1045–58. https://doi.org/10.1007/s10973-019-08007-z.
56. Hajatzadeh Pordanjani A, et al. Investigation of free convection heat transfer and entropy generation of nanofluid flow inside a cavity affected by magnetic field and thermal radiation. J Therm Anal Calorim. 2019;137(3):997–1019. https://doi.org/10.1007/s10973-018-7982-4.
57. Ahmadi B, et al. Energy and exergy analysis and optimization of a gas turbine cycle coupled by a bottoming organic Rankine cycle. J Thermal Anal Calorimet. 2019. https://doi.org/10.1007/s10973-019-09088-6.
58. Praprotnik M, et al. Temperature dependence of water vibrational spectrum: a molecular dynamics simulation study. J Phys Chem A. 2004;108(50):11056–62. https://doi.org/10.1021/jp046158d.
59. Barnoon P, et al. Application of rotating circular obstacles in improving ferrofluid heat transfer in an enclosure saturated with porous medium subjected to a magnetic field. J Therm Anal Calorim. 2020. https://doi.org/10.1007/s10973-020-09896-1.
60. Jones JE. On the determination of molecular fields.—II. From the equation of state of a gas. Proc R Soc Lond Ser A Contain Papers Math Phys Charact. 1924;106(738):463–77. https://doi.org/10.1098/rspa.1924.0082.
61. Varzaneh AA, et al. Comprehensive simulation of nanofluid flow and heat transfer in straight ribbed microtube using single-phase and two-phase models for choosing the best conditions. J Therm Anal Calorim. 2020;139(1):701–20. https://doi.org/10.1007/s10973-019-08381-8.
62. Peng Y, et al. Investigation of energy performance in a U-shaped evacuated solar tube collector using oxide added nanoparticles through the emitter, absorber and transmittal environments via discrete ordinates radiation method. J Therm Anal Calorim. 2020;139(4):2623–31. https://doi.org/10.1007/s10973-019-08684-w.
63. Tersoff J. New empirical approach for the structure and energy of covalent systems. Phys Rev B. 1988;37(12):6991. https://doi.org/10.1103/PhysRevB.37.6991.
64. Nguyen Q et al. Discrete Ordinates thermal radiation with mixed convection to involve nanoparticles absorption, scattering and dispersion along radiation beams through the nanofluid. J Therm Anal Calorim. 2020.
65. Zheng Y, et al. Free convection/radiation and entropy generation analyses for nanofluid of inclined square enclosure with uniform magnetic field. J Therm Anal Calorim. 2020. https://doi.org/10.1007/s10973-020-09497-y.
66. Green Melville S. Markoff random processes and the statistical mechanics of time-dependent phenomena. II. Irreversible processes in fluids. J Chem Phys. 1954;22(3):398–413. https://doi.org/10.1063/1.1740082.
67. He W, et al. Controlled elitist multi-objective genetic algorithm joined with neural network to study the effects of nano-clay percentage on cell size and polymer foams density of PVC/clay nanocomposites. J Therm Anal Calorim. 2020;139(4):2801–10. https://doi.org/10.1007/s10973-019-09059-x.
68. Wu H, et al. Heat transfer analysis of energy and exergy improvement in water-tube boiler in steam generation process. J Therm Anal Calorim. 2020;139(4):2791–9. https://doi.org/10.1007/s10973-019-09034-6.